Comparing Cone Beam Laminographic System Trajectories for Composite NDT

Neil O'Brien[a,*], Mark Mavrogordato[a], Richard Boardman[a], Ian Sinclair[a], Sam Hawker[c], Thomas Blumensath[a,b]

[a] µ-VIS X-Ray Imaging Centre, University of Southampton, Highfield, Southampton, UK SO17 1BJ, e-mail: nsob1c12@soton.ac.uk (*corresponding author), mnm100@soton.ac.uk, rpb@soton.ac.uk, is1@soton.ac.uk

[b] ISVR, University of Southampton, Highfield, Southampton, UK SO17 1BJ, e-mail: Thomas.Blumensath@soton.ac.uk

[c] Nikon Metrology UK Limited, Tring Business Park, Icknield Way, Tring UK HP23 4JX, e-mail: Sam.Hawker@nikon.com

Abstract
We compare the quality of reconstruction obtainable using various laminographic system trajectories that have been described in the literature, with reference to detecting defects in composite materials in engineering. We start by describing a laminar phantom representing a simplified model of composite panel, which models certain defects that may arise in such materials, such as voids, resin rich areas, and delamination, and additionally features both blind and through holes along multiple axes. We simulate ideal cone-beam projections of this phantom with the different laminographic trajectories, appling both Simultaneous Iterative Reconstruction Technique (SIRT) and Conjugate Gradient Least Squares (CGLS) reconstruction algorithms. We compare the quality of the reconstructions with a view towards optimising the scan parameters for defect detectability in composite NDT applications.

Keywords: Computed Laminography, Cone-beam, Composites, NDT, acquisition trajectories

1 Introduction

X-ray computed tomography (CT) is a widely accepted and applied method for non-destructive testing in the engineering community, applied across research and development, quality control, and post-failure analysis for engineered components. Since its introduction, the technique has been refined and developed considerably, with typical detector arrays improving from 80x80 pixels in the early days [1] to the order of several thousand pixels square today. Meanwhile, the introduction of new algorithms and computational techniques, such as general-purpose use of the graphics processing unit (GPGPU), has dramatically accelerated and enhanced the reconstruction process. By their nature, polymer matrix composites are widely used in planar forms in structural applications [2]. Whilst traditional micro-focus CT can provide high-resolution 3D visualisation of the structure of relatively small composite parts with aspect ratios that maintain broadly similar path lengths in all orientations during a scan, larger composite panels are less readily examined due to the limited space within a typical CT scanner and the likelihood of near-extinction of the X-ray beam along the long axis/plane of the sample, leading to photon starvation and artefacts in the reconstructed volume.

Several solutions to the problem of scanning larger composite panels and those with unfavourable aspect ratios have been explored, including dual-energy scanning using higher energies for the orientations with longer path-lengths [3], and stacking samples within one CT scan to achieve more uniform path length and thus attenuation at all angles. A futher key solution for imaging large planar composites is to use computed laminography (CL), which may employ any of several acquisition trajectories, combined with any of various reconstruction methods, many of which are adapted from CT. In avoiding a complete rotation of the sample in question, CL captures only a limited subset of the data that an ideal CT scan would contain, but makes feasible scans outside the scope of full CT. By utilising *a priori* knowledge in the reconstruction algorithm, high quality volume inspection is possible [4]. CL has been in use at synchrotron facilities for some time [5] and there is growing interest in cone beam laminography [6] which is practical using compact, laboratory-based sources.

In this paper we will introduce a phantom to represent a simplified composite sample with various defects, illustrate several laminographic system trajectories, and by comparing line-profiles through various reconstructions of the phantom, compare the quality of the results.

2 Description of Phantom, Acquisition Trajectories and Simulation Techniques

Our phantom consists of a cuboid, which measures 70.7 x 70.7 x 4mm with a 100µm voxel size. Simplified defects of interest in large engineering applications are modelled: we include through- and blind-holes along three axes as well as resin-rich areas of 100µm and 300µm thickness, and a delamination modelled as an air layer of 100µm thickness on the central plane. We also included several smaller voids, ranging in size from a cube with 100µm side length to a cuboid 200µm x 200µm x 1mm. We adopted the elemental composition of the carbon fibre bundles and the epoxy from values given by Bliznakova *et al.* [7]; using the attenuation data from the NIST database, we set the relative attenuations of the various parts of the phantom to 0.767 for the

bulk material, 0.726 for the epoxy in the resin-rich regions, and 0 for the air regions. Whilst the features are spread throughout the thickness (*z*-axis) of the planar phantom, we show all features in a *z*-projection in Figure 1.

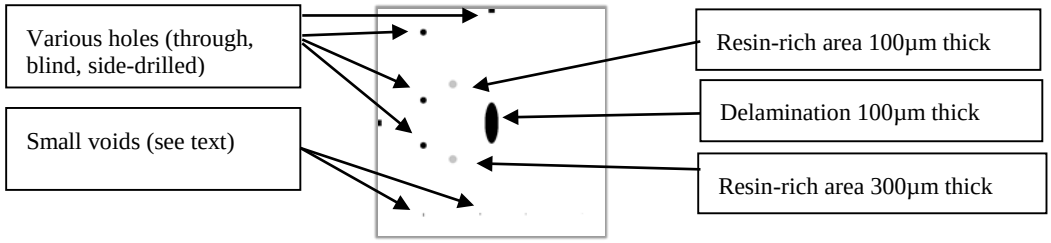

Figure 1: Schematic layout of the phantom

2.1 Trajectories implemented

The simulated trajectories are illustrated schematically in Figure 2. We varied some of the parameters for each motion (*e.g.* the angular range covered on each axis in the swing/limited-angle setup; the angle between the principal ray and the axis of rotation for the rotary configuration). We also considered both single- and double-sided illumination of the phantom, which could be implemented in a real system by several means including repositioning the sample relative to a source-detector pair, or potentially using multiple source-detector pairs.

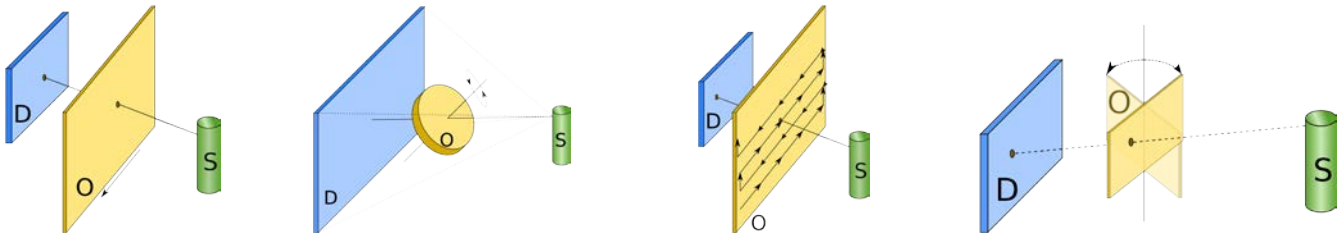

Figure 2: Schematics of the scan trajectories we considered, from left to right: linear, rotary, linear raster, and swing or limited-angle (one axes of rotation is shown).

2.2 Simulation techniques

We applied the ASTRA toolkit [8] which provides a number of routines for tomographic simulation and reconstruction development, including GPU-accelerated cone-beam forward projection and iterative reconstruction algorithms for arbitrary cone-beam acquisition geometries. We used both the SIRT and CGLS reconstruction methods as implemented in the ASTRA toolbox with a range of different iteration counts. We compare the line profiles recorded through certain features in our phantom with those through the reconstructed volumes for our chosen scan trajectories, in order to evaluate the relative merits of each method to reveal flaws in laminar specimens. The simulations presented here take several simplifying assumptions including assuming a monochromatic point source, as well as not adding any artificial noise or detector faults to the simulated results.

3 Results and Discussion

3.1 Influence of Trajectory Type

In Figure 3, we present line profiles through our phantom as well as through the reconstructed volume for each of the trajectories illustrated in Section 2.1. These results are all based on SIRT reconstructions using 15 iterations, and take a line profile across the through hole feature, approximately 1/3 through the thickness of the volume. It can be seen that whilst all trajectories considered correctly reproduce the zero attenuation in the centre, the linear and raster trajectories have bright artefacts around the edge of the hole. The rotary trajectory does not give rise to a bright artefact, but suffers from the slowest gradient in grey-value across the edge of the feature.

3.2 Influence of reconstruction parameters

In Figure 4, we show line profiles through the second blind hole in our phantom, half-way down its depth. We compare the results for different iteration counts and reconstruction algorithms using the same projections, from our limited-angle simulation using two-sided scanning and a 2-axis swing motion between ±45° about both axes. The overall feature contrast improves when increasing the iteration count, but the additional iterations also exacerbate the bright artefact arising at the edges of the hole. SIRT reconstructs the greyvalues of the phantom correctly in more places than CGLS but both methods produce a good qualitative match to the phantom. We note that for the detection of voids in an NDE application, this type of artefact may not pose a problem, but increasing iteration counts still incur the tradeoff of requiring increased processing time.

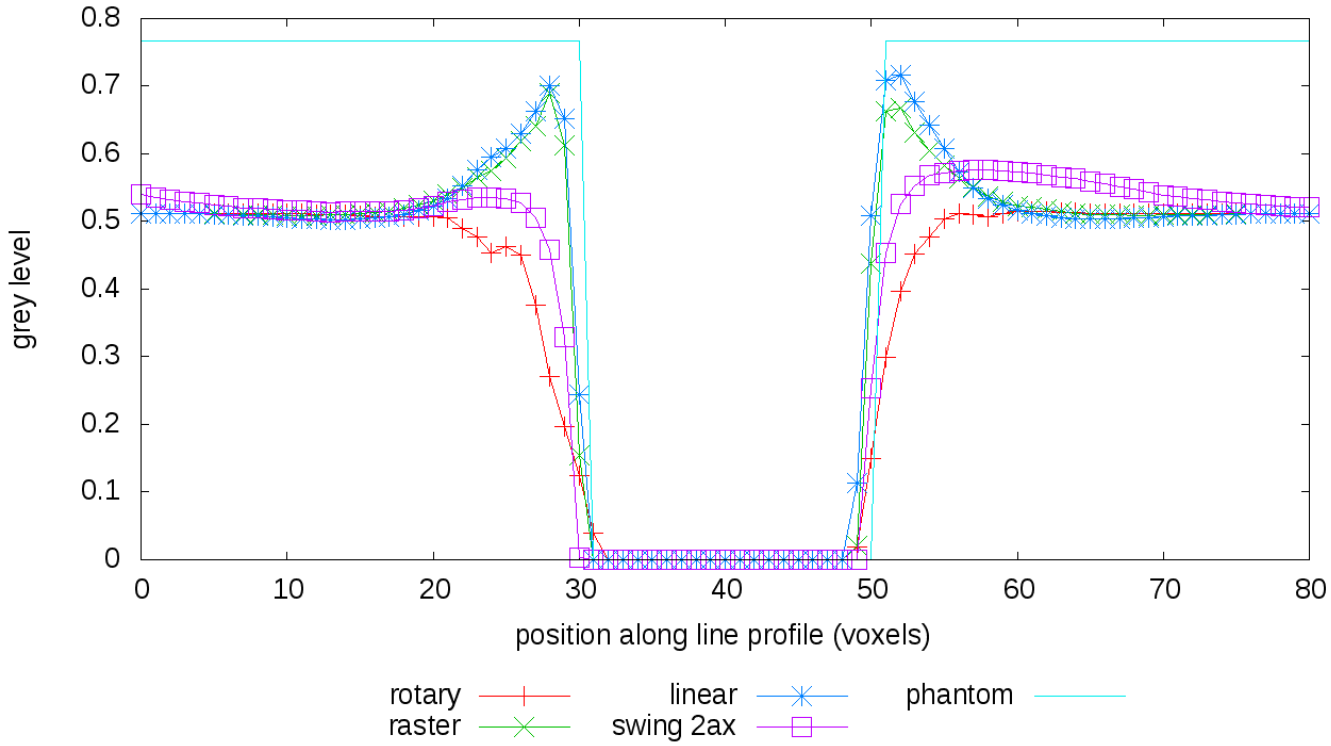

Figure 3: line profiles across through hole in *x*-direction for several trajectory types. Note that "swing 2ax" refers to the swing/limited-angle laminographic trajectory in which the specimen is rotated simultaneously about two perpendicular axes that cross at its centre. All results presented used 15 SIRT iterations and illuminated the specimen from one side only.

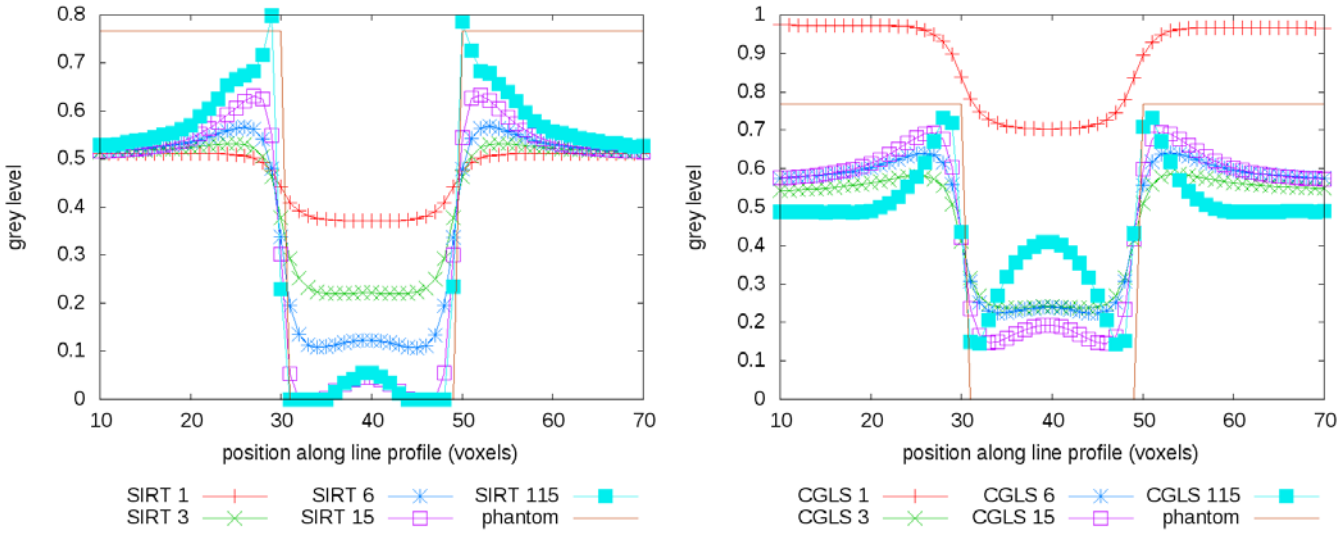

Figure 4: profiles along the y-direction of a blind hole in the reconstruction for various numbers of iterations of the SIRT (left) and CGLS (right) iterative reconstruction techniques. All results are from a 2-sided, 2-axis swing simulation using angular limits of ±45°. All output volumes were scaled such that the floating-point values were in the range [0,1] prior to taking the line profiles, ensuring comparability.

3.3 Influence of trajectory parameters

In this subsection we investigate the influence of some of the variable parameters of the various trajectories, such as the total range of motion that the specimen is subjected to. Figure 6 compares raster scans for different total displacements; the cone-beam illuminates all parts of the phantom from a range of angles; with larger displacements, the outer edges of the phantom are illuminated by the rays over a smaller range of angles than with smaller displacement values, improving the definition.

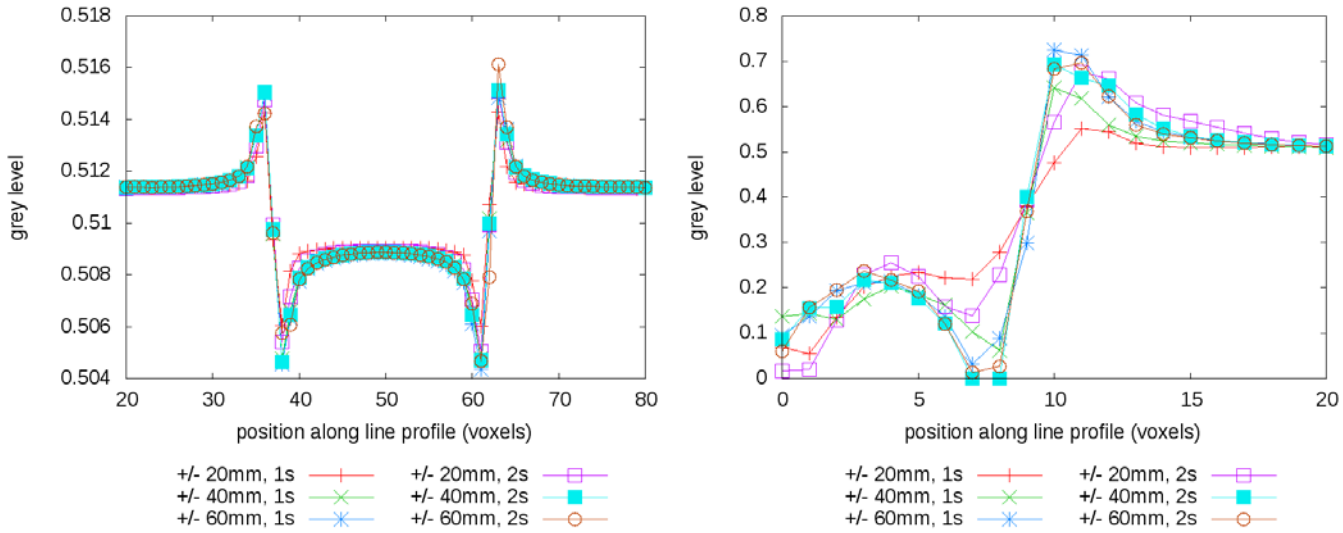

Figure 6: Profiles along the *x*-direction through a resin-rich region (left plot) and side hole (right plot), showing influence of different total amounts of displacement and the difference between 1-sided (1s) and 2-sided (2s) scanning.

3.4 Slice images

In figure 7 we illustrate a slice through our raster-scan reconstruction on the left hand side and a section view of a swing scan on the right hand side, showing that the defects can be localised to an approximate depth in the plane but that the depth resolution is strongly improved in the swing trajectory by using a larger angular range.

4 Discussion and Conclusions

We have compared the ability of various laminographic trajectories to discern the features of our phantom; all the methods show promising results and those illuminating features from a larger range of angles typically give better resolution. The choice of reconstruction algorithm and iteration count is shown to be important; SIRT has provided results in better agreement with the phantom in these simulations, and for these data, 15 iterations achieves good feature definition without costing excessive compute time. In a real system we suggest that the iteration count should be decided empirically to optimise performance for specific acquisition setups.

Acknowledgements

The authors gratefully acknowledge funding for ProjectCAN from Innovate UK, the UK's innovation agency through TSB grant 101804. The ProjectCAN consortium of QinetiQ, University of Southampton, University College London, Nikon, Axi-Tek, and Rolls Royce brings together world leaders from academia, the aerospace industry, and X-ray equipment manufacture. The simulations reported upon here have been discussed with consortium partners but the analysis and reporting of results was carried out entirely by the authors. The authors also acknowledge the use of the IRIDIS High Performance Computing Facility at the University of Southampton in the completion of this work.

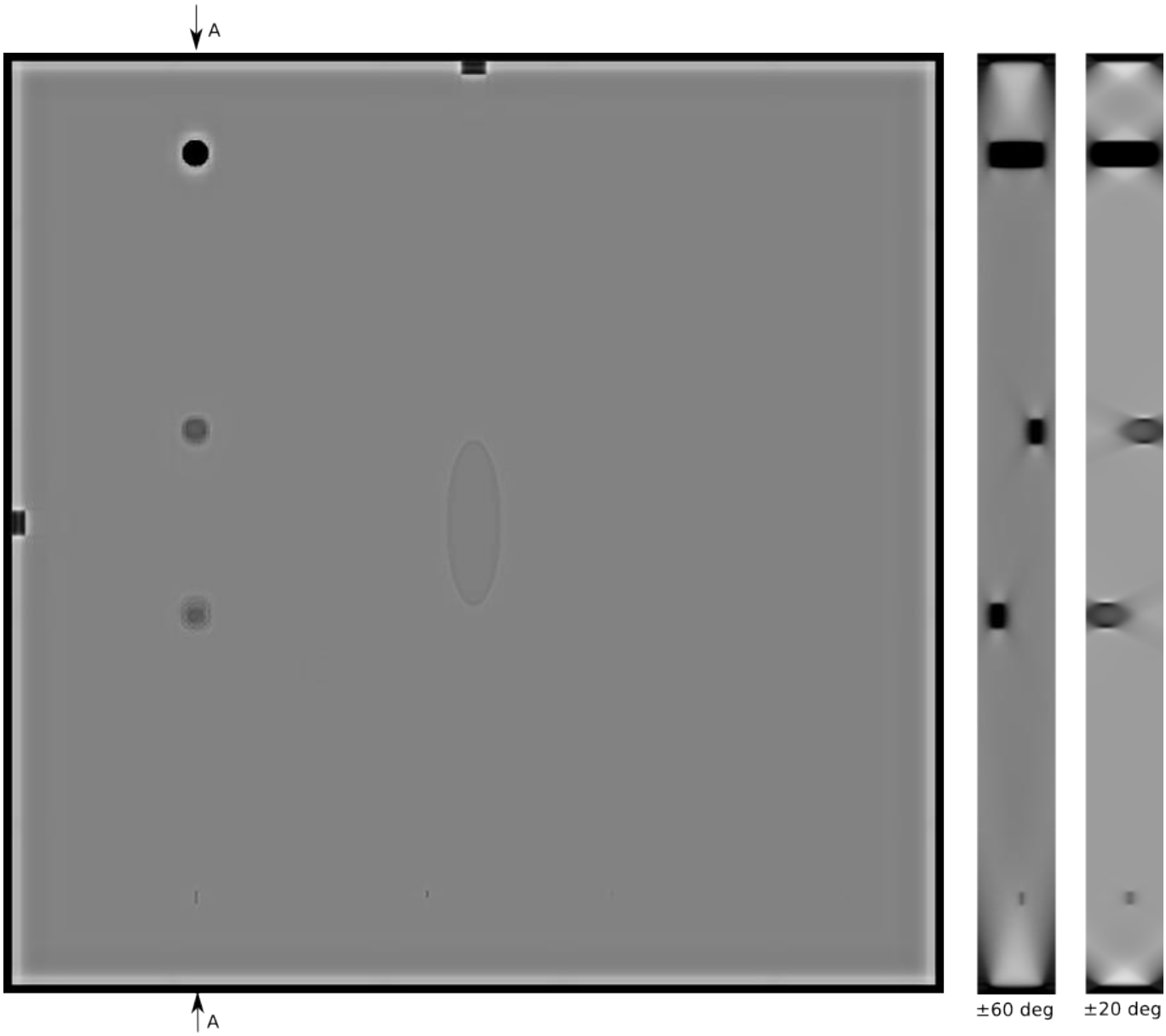

Figure 7: (left) a slice through a 2-sided raster scan with 15 iterations of SIRT reconstruction showing reconstruction of central void, small voids, and various holes; (right) slices through the thickness taken from 2-axis, 2-sided swing simulations using showing localisation of various defects in the thickness of the slice.

References

[1] E. C. Beckmann, “CT scanning: the early days”, British J. Radiology, vol. 79, no. 937, 2006

[2] D. Bull, L. Helfen, I. Sinclair, S. M. Spearing, “Multi-scale 3D Imaging of Carbon Fibre Laminate Impact and Compression After Impact Damage Using Computed Tomography and Laminography”, ECCM15 - 15th European Conference on Composite Materials, Venice, Italy, June 2012.

[3] J. E. Rouse, “Characterisation of Impact Damage in Carbon Fibre Reinforced Plastics by 3D X-Ray Tomography”. PhD thesis, University of Manchester, Manchester, UK, 2012

[4] L. Helfen, A. Myagotin, P. Mikulík, P. Pernot, A. Voropaev, M. Elyyan, M. Di Michiel, J. Baruchel, T. Baumbach, “On the implementation of computed laminography using synchrotron radiation”, Review of Scientific Instruments, vol 82, no. 6, 2011

[5] L. Helfen, F. Xu, H. Suhonen, P. Cloetens, T. Baumbach, “Laminographic imaging using synchrotron radiation – challenges and opportunities,” Journal of Physics: Conference Series, vol. 425, no. 19, page 192025, 2013.

[6] N. S. O'Brien, R. P. Boardman, I. Sinclair, T. Blumensath, “Recent advances in X-ray cone-beam computed laminography”, Journal of X-Ray Science and Technology, submitted.

[7] K Bliznakova, A Dermitzakis, Z Bliznakov, Z Kamarianakis , I Buliev and N Pallikarakis, “Modeling of small carbon fiber-reinforced polymers for X-ray imaging simulation”, J. Composite Materials, September 2014.

[8] W. van Aarle, W. J. Palenstijn, J. De Beenhouwer, T. Altantzis, S. Bals, K J. Batenburg, and J. Sijbers, "The ASTRA Toolbox: A platform for advanced algorithm development in electron tomography", Ultramicroscopy, Vol 157, pages 35-47, 2015.